Topological Transition of Dirac Points in a Microwave Experiment

Matthieu Bellec,[1] Ulrich Kuhl,[1] Gilles Montambaux,[2] and Fabrice Mortessagne[1,*]

[1]*Laboratoire Physique de la Matière Condensée, CNRS UMR 7336, Université Nice-Sophia Antipolis, 06100 Nice, France*
[2]*Laboratoire de Physique des Solides, CNRS UMR 8502, Université Paris-Sud, 91405 Orsay Cedex, France*
(Received 17 October 2012; published 14 January 2013)

By means of a microwave tight-binding analogue experiment of a graphenelike lattice, we observe a topological transition between a phase with a pointlike band gap characteristic of massless Dirac fermions and a gapped phase. By applying a controlled anisotropy on the structure, we investigate the transition directly via density of states measurements. The wave function associated with each eigenvalue is mapped and reveals new states at the Dirac point, localized on the armchair edges. We find that with increasing anisotropy, these new states are more and more localized at the edges.

Introduction.—Recently discovered condensed matter systems, such as graphene [1] or topological insulators [2], constitute an ideal playground to investigate the physics of massless Dirac fermions until now restricted to high energy physics. Indeed, the relativistic spectrum emerges at the conical intersection points, the so-called Dirac points, in the low energy electronic dispersion relation. The large potential of technological applications [3] depends crucially on the properties of these quasiparticles. The manipulation of the Dirac points by external parameters—from creation to annihilation—has recently attracted significant attention both theoretically [4–7] and experimentally [8,9]. By controlling the anisotropy of a honeycomb lattice, one can in principle move the Dirac points up to a transition where they merge and annihilate each other. This is a topological transition since both Dirac points are characterized by opposite topological numbers (opposite Berry phases) which annihilate at the transition. If the anisotropy is increased further, a band gap opens in the dispersion relation. This transition from a gapless (Dirac) phase to a gapped phase corresponds to a Lifshitz phase transition from a semimetallic to an insulating phase [4–7]. The experimental investigation of this transition is difficult to perform with condensed matter systems, e.g., graphene under uniaxial strain [10] or quasi-two-dimensional organic conductors under pressure [11]. Artificial systems such as molecular graphene or ultracold atoms in optical lattices have been recently proposed to experimentally probe this topological transition [8,9]. While this effect has not been clearly observed with molecular graphene [9], Ref. [8] reports the observation, using momentum-resolved interband transitions, of Dirac points merging with a Fermi gas in an anisotropic honeycomb lattice without sixfold symmetry.

Alternatively, discrete photonic systems (e.g., photonic lattices or microwave cavities), with graphenelike structures, have been employed as condensed-matter analogues [12–15]. In microwave experiments, the tight-binding form of graphene's Hamiltonian [16] can be established by using a honeycomb lattice of evanescently coupled dielectric resonators [14,15]. Dirac points and signature of the linear dispersion relation have been observed [13–15].

In this Letter, we take advantage of the high versatility of our tight-binding microwave setup to explore the topological phase transition. The anisotropy of the honeycomb lattice is controlled through the nearest-neighbor hopping parameters. We directly measure the density of states (DOS) and the wave function associated with each eigenvalue. We observe a transition between the Dirac phase and the gapped phase exactly for the expected value of the anisotropy parameter defined in a tight-binding description. This is the first direct DOS measurement of this topological transition. Moreover the experimental setup allows a very fine manipulation of the edges and a control of edge states that is not yet possible in condensed matter systems. We show that the anisotropy generates new states, at the Dirac frequency ν_D, localized along specific armchair edges. With increasing anisotropy, their extension into the bulk decreases.

Experimental microwave graphene analogue.—For our experiments, we use a set of 222 identical coupled dielectric cylindrical resonators (5 mm height, 8 mm diameter, and a refractive index of 6), hereafter called *discs*, placed in between two metallic plates. We establish a two-dimensional tight-binding regime, where the electromagnetic field is mostly confined within the discs and spreads out evanescently. The experimental details are described in Refs. [14,15]. Via a movable loop-antenna, the reflected signal S_{11} is measured over a given frequency range at the disc positions **r** using a vectorial network analyzer. The bare frequency ν_0 of an isolated disc (~ 6.65 GHz in the setup considered here) corresponds to the on-site energy appearing in the tight-binding Hamiltonian. The coupling parameter t_{exp} between two adjacent discs depends on the disc separation d and can be described, as expected for a two-dimensional system, by a modified Bessel function K_0 (see Table I). Thus, by changing the distance between discs, one can change, in a controllable manner, the

TABLE I. Experimental anisotropy parameter $\beta = t'_{exp}/t_{exp}$. For the regular lattice (i.e., $\beta = 1$), $d = 15$ mm and $t_{exp} = 0.016$ GHz. The intersite distances d' and the corresponding nearest-neighbor coupling values βt_{exp} are also indicated.

d' (mm)	βt_{exp}[a] (GHz)	β
15.0	0.015	1
13.9	0.020	1.3
13.0	0.027	1.8
12.6	0.030	2
12.0	0.037	2.5
11.0	0.053	3.5

[a]Obtained according to the Bessel fit $t_{exp}(d) = \alpha|K_0(\gamma d/2)|^2 + \delta$. $\alpha = 1.9545$ GHz, $\gamma = 0.3167$ mm^{-1} and $\delta = 0.0049$ GHz have been experimentally determined [17].

intersite couplings. For a lattice composed of many discs, the setup allows for direct access to the local density of states through the measured quantity S_{11} [14,15]. The DOS is obtained by averaging over all positions $\mathbf{r}$. Moreover, our setup allows us to visualize the wave function associated with each eigenfrequency [17].

Tight-binding description.—In order to interpret quantitatively our experimental results, we present a tight-binding model on an infinite hexagonal lattice with first, second, and third nearest-neighbor couplings. The on-site "energy" is given by the bare frequency ν_0. The hopping amplitudes (in units of frequency) between nearest-neighbor sites are called t' along the y axis and t along the other directions [respectively, red and blue links on Fig. 1(a)]. The next- (next-) nearest-neighbor couplings are respectively denoted as t_2 and t_3. The anisotropy of the lattice can be simply taken into account via the first nearest-neighbor coupling (i.e., t'), and higher-order terms are assumed to be unchanged (i.e., $t_2 = t'_2$ and $t_3 = t'_3$). In the basis of the two inequivalent sites forming the elementary cell, the Hamiltonian can be written in the Bloch representation,

$$\mathcal{H}_{TB} = \begin{pmatrix} \nu_0 + f_2(\mathbf{k}) & f(\mathbf{k}) + f_3(\mathbf{k}) \\ f^*(\mathbf{k}) + f^*_3(\mathbf{k}) & \nu_0 + f_2(\mathbf{k}) \end{pmatrix}, \quad (1)$$

where f (respectively, f_2 and f_3) is the first (respectively, second and third) nearest-neighbor contribution, $f(\mathbf{k}) = -(t' + te^{i\mathbf{k}\cdot\mathbf{a}_1} + te^{i\mathbf{k}\cdot\mathbf{a}_2})$, respectively $f_2(\mathbf{k}) = -2t_2[\cos\mathbf{k}\cdot\mathbf{a}_1 + \cos\mathbf{k}\cdot\mathbf{a}_2 + \cos\mathbf{k}\cdot(\mathbf{a}_1 - \mathbf{a}_2)]$, and $f_3(\mathbf{k}) = -t_3[e^{i\mathbf{k}\cdot(\mathbf{a}_1+\mathbf{a}_2)} + e^{i\mathbf{k}\cdot(\mathbf{a}_1-\mathbf{a}_2)} + e^{i\mathbf{k}\cdot(\mathbf{a}_2-\mathbf{a}_1)}]$. The frequency spectrum is given by $\nu(\mathbf{k}) = \nu_0 + f_2(\mathbf{k}) \pm |f(\mathbf{k}) + f_3(\mathbf{k})|$ and consists of two bands touching at the Dirac frequency $\nu_D = \nu_0 + 3t_2$. The corresponding DOS are represented in Fig. 1 for different values of the anisotropy parameter $\beta = t'/t$. For $\beta = 1$, two Dirac cones exist in k space at $\mathbf{k} = \pm\mathbf{K}_D = \pm(\mathbf{a}^*_1 - \mathbf{a}^*_2)/3$, where $\mathbf{a}^*_i$ are reciprocal lattice vectors. For larger β, the Dirac points move along the k_x axis. A topological transition occurs at
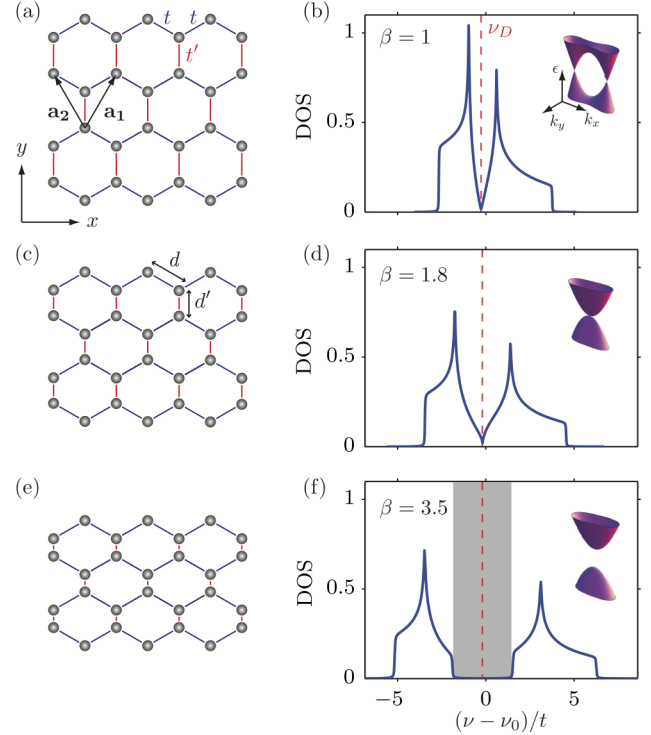

FIG. 1 (color online). Left panels: Schematics of the hexagonal lattices. $\mathbf{a}_1$ and $\mathbf{a}_2$ define the primitive cell of the Bravais lattice. t (blue intersite links) and t' (red ones, along y axis) correspond to the nearest-neighbor couplings. d and d' are the corresponding distances. An anisotropy is introduced along the y axis: t' increases when d' decreases. Right panels: Calculated density of states (DOS) for an infinite system with first, second, and third nearest-neighbor couplings given in the text. The red dashed line is the Dirac frequency $\nu_D = \nu_0 + 3t_2$. The insets show the corresponding dispersion relation. (a)–(b) Regular honeycomb lattice, $\beta = 1$. The two Dirac points are distinguishable. (c)–(d) Compressed lattice at the topological transition, $\beta = 1.8$. The Dirac points merge. (e)–(f) $\beta = 3.5$, a band gap opens (gray zone).

$\beta_c = 2 - 3t_3/t$, where the two Dirac points coalesce [inset Fig. 1(d)]. With the values of the coupling parameters extracted from the experiments (see below), we find $\beta_c = 1.8$. For β larger than this critical value, the condition $\nu(\mathbf{K}_D) = \nu_D$ cannot be fulfilled: a gap opens [inset Fig. 1(f)]. As a consequence, the density of states is strongly affected. The typical linear relation at the vicinity of the Dirac point (red dashed line) observed for $\beta = 1$ [Fig. 1(b)] turns to a square root law at the transition [Fig. 1(d)] [4,6]. Then a gap opens for $\beta > \beta_c$ [gray zone in Fig. 1(f)]. Note that next- (next-) nearest-neighbor couplings lead to (i) a lower value of β_c for the transition (1.8 instead of 2 expected when only the first nearest-neighbor coupling is taken into account [4,6]), (ii) an asymmetry of the bands, (iii) a slight shift of ν_D towards lower frequency, and (iv) a displacement of the two logarithmic singularities.

Topological transition and gap opening.—Experimentally, we first realize a regular graphene lattice

with an hexagonal shape which has only armchair bounda-
ries in order to eliminate edge states [see inset Fig. 2(a)].
We gradually add an anisotropy by increasing the coupling
t'_{exp} along the y axis—i.e., by decreasing the separation d'
between the discs along y (insets in Fig. 2). As detailed in
Table I, the anisotropy parameter β varies from 1 to 3.5.
The DOS corresponding, respectively, to $\beta = 1$, 1.8 ,3.5
are depicted in Fig. 2. For the regular graphene, for which
$d = d' = 15$ mm, the nonsymmetric band structure and
the pointlike gap at the Dirac frequency ν_D are observed
[Fig. 2(a)]. Here, due to the finite size of the system, the
expected linear behavior of the DOS near the Dirac point
appears only as a dip in the histogram. Moreover, the two
logarithmic singularities have their signature in this finite
sample (Fig. 2). By adjusting the calculated DOS shown
in Fig. 1(b) to the experimental one [17], the following
values for the three tight-binding coupling parameters are
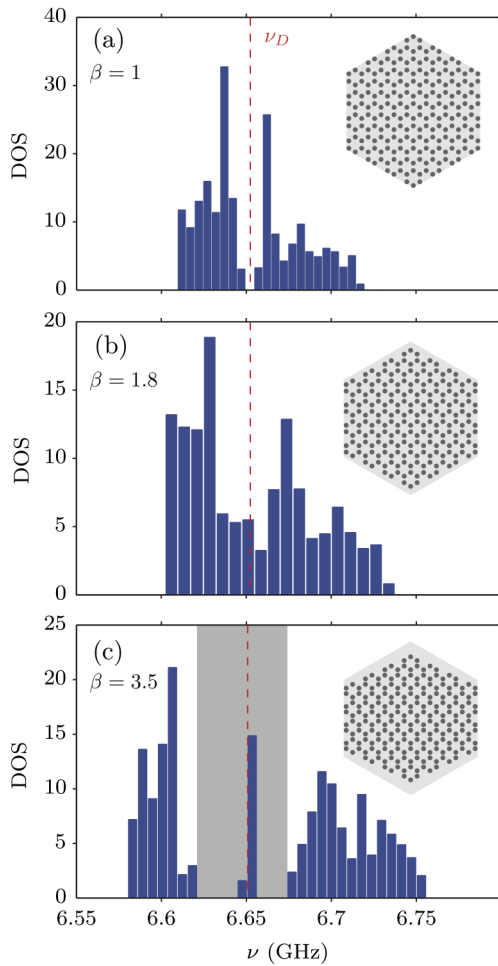obtained: $t = 0.016$ GHz, $t_2/t = -0.091$, and $t_3/t = 0.071$.

This value of t is in agreement with the Bessel fit of the
experimental coupling (see Table I).

Figures 2(b) and 2(c) show the evolution of the DOS
when the lattice is compressed. For large values of β, a gap
opens as expected but additional states appear around ν_D.
We will provide a description of these states, identified as
edge states, in the last part of the Letter. For an inspec-
tion of the topological transition, we eliminate their con-
tributions by averaging the signal over bulk sites only. In
Fig. 3(a), we plot the measured DOS obtained for six
different values of β using a white-blue color scale. The
dashed red line corresponds to the Dirac frequency and
the gray zone is used here to improve the visualization
of the band gap opening. These experimental results are
successfully compared with the DOS calculated for the
corresponding infinite systems [Fig. 3(b)]. We clearly
distinguish the topological transition between a gapless
phase and a gapped phase which occurs for $\beta_c = 1.8$, as
expected from the theoretical expression $\beta_c = 2 - 3t_3/t$
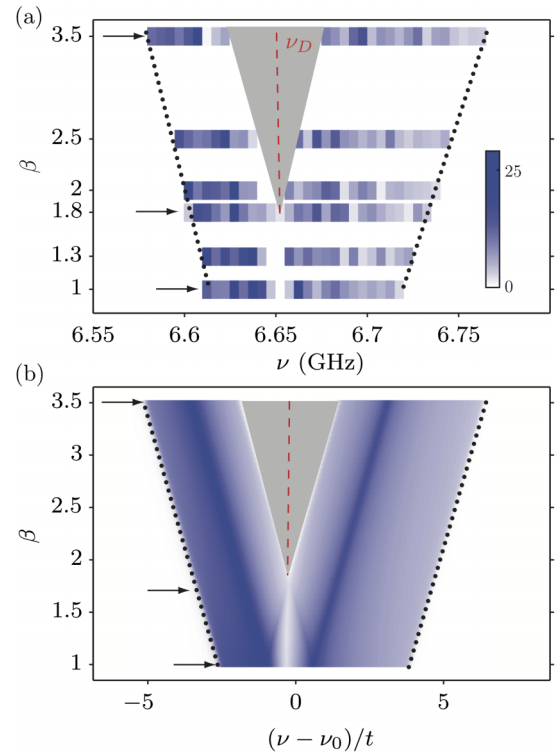and the tight-binding parameters given above. Before the

FIG. 2 (color online).   Experimental DOS for (a) the regular
graphene $(\beta = 1)$, (b) and (c) anisotropic structures with
$\beta = 1.8$ and $\beta = 3.5$, respectively. The dashed red lines indicate
the Dirac frequency ν_D. The gray zone shows the band gap with
edge states at ν_D.

FIG. 3 (color online).   (a) Experimental DOS for β varying
from 1 to 3.5. To remove edges states and highlight the band gap
opening, the DOS have been averaged over bulk sites only. The
arrows at $\beta = 1$, 1.8, and 3.5 indicate the DOS plotted, respec-
tively, in Figs. 2(a)–2(c), where the average was performed over
all sites. (b) Calculated DOS for β varying from 1 to 3.5 for an
infinite system. The arrows at $\beta = 1$, 1.8, and 3.5 indicate the
DOS plotted in Figs. 1(b), 1(d), and 1(f), respectively. In (a) and
(b), the gray zone shows the band gap opening, the dotted lines
denote the linear dependence of the band edges, and the red
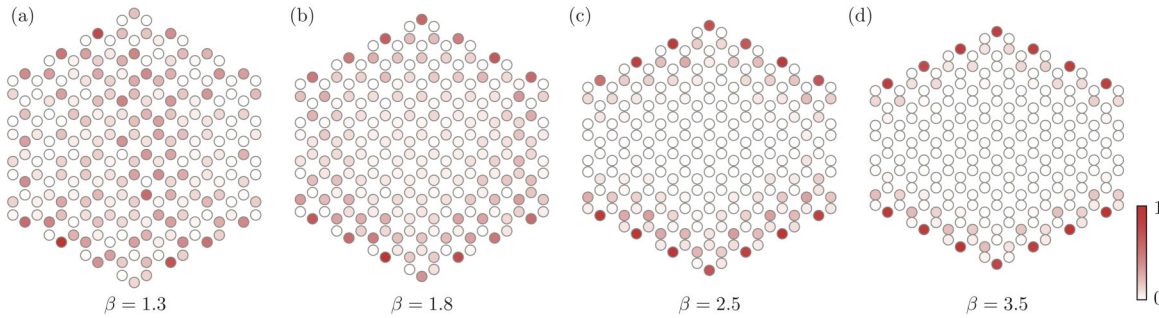dashed line indicates ν_D.

FIG. 4 (color online). Experimental wave function distributions at the Dirac frequency ν_D (red dashed line in Fig. 3) for β ranging from 1.3 to 3.5.

transition, the spectrum exhibits a pointlike gap. At the transition, since the DOS close to the Dirac point is supposed to switch from a linear to a square root behavior [4,6], the number of states close to the Dirac point is expected to increase. Due to the finite size of the lattice, a small gap always exists, but a higher concentration of states at ν_D is clearly seen, which reveals the topological phase transition. Finally, above the transition a gap opens. The gap and the bandwidths linearly increase with β (respectively, the gray zone and the dotted lines in Fig. 3).

Edge states.—We now focus on the states that appear at the Dirac frequency ν_D for anisotropic lattices (see Fig. 2). The spatial distribution of these states is depicted in Fig. 4, where it appears clearly that they are indeed edge states, which may appear *a priori* surprising since armchair boundaries are not expected to support edge states [18]. Their structure will be carefully studied in a future work, but the following remarks are of immediate interest in this Letter: (i) Edge states appear only along the edges that are not parallel to the anisotropy axis. (ii) Their localization along the edge increases when β increases. (iii) Their existence is not related to the topological transition observed in Fig. 3: they appear as soon as $\beta > 1$. These features are in agreement with the prediction for the existence of armchair edge states in deformed structures [19]. Moreover, we find that (i) the intensity on one triangular sublattice stays zero, and (ii) the intensity on the other sublattice decreases roughly as $(1/\beta)^{2r}$, where r is the distance to the edge in units of the lattice parameter. A more extensive investigation of these states, as well as of the states along zig-zag and bearded edges in anisotropic structures, is in progress.

Conclusion.—To conclude, we have exploited the high flexibility of a microwave two-dimensional analogue of strained graphene to experimentally demonstrate the existence of a topological transition between a gapless phase and a gapped phase when the anisotropy increases. We have investigated the spectral properties of this structure by directly measuring the density of electromagnetic modes. An appropriate description of this system requires us to take into account not only first but also next- (next-) nearest-neighbor couplings. The wave functions associated with the states appearing at the Dirac frequency are easily measurable with our setup, and they reveal the presence of edge states along the armchair edges. They become more and more localized along the edges as the anisotropy is increased. Finally, the versatility of the setup allows us to mimic many of the spectacular properties of graphene and to reveal many other physical phenomena, such as the influence of pseudo-magnetic fields and associated Landau levels induced by a specific strain in graphenelike lattices [20].

*fabrice.mortessagne@unice.fr

[1] A. C. Neto, F. Guinea, N. Peres, K. Novoselov, and A. Geim, Rev. Mod. Phys. **81**, 109 (2009).
[2] M. Hasan and C. Kane, Rev. Mod. Phys. **82**, 3045 (2010).
[3] For graphene, see a recent outlook in H. Brody, Nature (London) **483**, S29 (2012).
[4] Y. Hasegawa, R. Konno, H. Nakano, and M. Kohmoto, Phys. Rev. B **74**, 033413 (2006).
[5] S.-L. Zhu, B. Wang, and L.-M. Duan, Phys. Rev. Lett. **98**, 260402 (2007); B. Wunsch, F. Guinea, and F. Sols, New J. Phys. **10**, 103027 (2008); K. L. Lee, B. Grémaud, R. Han, B.-G. Englert, and C. Miniatura, Phys. Rev. A **80**, 043411 (2009).
[6] G. Montambaux, F. Piéchon, J.-N. Fuchs, and M. O. Goerbig, Phys. Rev. B **80**, 153412 (2009); Eur. Phys. J. B **72**, 509 (2009).
[7] P. Dietl, F. Piéchon, and G. Montambaux, Phys. Rev. Lett. **100**, 236405 (2008).
[8] L. Tarruell, D. Greif, T. Uehlinger, G. Jotzu, and T. Esslinger, Nature (London) **483**, 302 (2012); L.-K. Lim, J.-N. Fuchs, and G. Montambaux, Phys. Rev. Lett. **108**, 175303 (2012).
[9] K. K. Gomes, W. Mar, W. Ko, F. Guinea, and H. C. Manoharan, Nature (London) **483**, 306 (2012).
[10] V. M. Pereira, A. H. C. Neto, and N. M. R. Peres, Phys. Rev. B **80**, 045401 (2009).
[11] S. Katayama, A. Kobayashi, and Y. Suzumura, J. Phys. Soc. Jpn. **75**, 054705 (2006); M. O. Goerbig, J.-N. Fuchs, G. Montambaux, and F. Piéchon, Phys. Rev. B **78**, 045415 (2008).
[12] O. Peleg, G. Bartal, B. Freedman, O. Manela, M. Segev, and D. N. Christodoulides, Phys. Rev. Lett. **98**, 103901 (2007).

[13] S. Bittner, B. Dietz, M. Miski-Oglu, P.O. Iriarte, A. Richter, and F. Schäfer, Phys. Rev. B **82**, 014301 (2010); S.R. Zandbergen and M.J.A. de Dood, Phys. Rev. Lett. **104**, 043903 (2010); S. Bittner, B. Dietz, M. Miski-Oglu, and A. Richter, Phys. Rev. B **85**, 064301 (2012).

[14] U. Kuhl, S. Barkhofen, T. Tudorovskiy, H.-J. Stöckmann, T. Hossain, L. de Forges de Parny, and F. Mortessagne, Phys. Rev. B **82**, 094308 (2010).

[15] S. Barkhofen, M. Bellec, U. Kuhl, and F. Mortessagne, Phys. Rev. B **87**, 035101 (2013).

[16] P.R. Wallace, Phys. Rev. **71**, 622 (1947); S. Reich, J. Maultzsch, C. Thomsen, and P. Ordejón, Phys. Rev. B **66**, 035412 (2002).

[17] M. Bellec, U. Kuhl, G. Montambaux, and F. Mortessagne (to be published).

[18] K. Nakada, M. Fujita, G. Dresselhaus, and M.S. Dresselhaus, Phys. Rev. B **54**, 17954 (1996).

[19] P. Delplace, D. Ullmo, and G. Montambaux, Phys. Rev. B **84**, 195452 (2011).

[20] F. Guinea, M. Katsnelson, and A. Geim, Nat. Phys. **6**, 30 (2010).